

# Deposition of high quality $\text{YBa}_2\text{Cu}_3\text{O}_{7-\delta}$ thin films over large areas by pulsed laser ablation with substrate scanning

M. F. Davis and J. Wosik

*Department of Electrical Engineering, Texas Center for Superconductivity, University of Houston, Houston, Texas 77204-4793*

K. Forster and S. C. Deshmukh

*Department of Chemical Engineering, Texas Center for Superconductivity, University of Houston, Houston, Texas 77204-4793*

H. R. Rampersad, S. Shah, P. Siemsen, and J. C. Wolfe

*Department of Electrical Engineering, Texas Center for Superconductivity, University of Houston, Houston, Texas 77204-4793*

D. J. Economou

*Department of Chemical Engineering, Texas Center for Superconductivity, University of Houston, Houston, Texas 77204-4793*

(Received 14 December 1990; accepted for publication 8 February 1991)

We describe the transport and structural properties of  $\text{YBa}_2\text{Cu}_3\text{O}_{7-\delta}$  thin films deposited by pulsed laser ablation with computer-controlled substrate scanning. Films were deposited on  $\text{LaAlO}_3$  and  $\text{SrTiO}_3$  substrates covering a  $2 \times 3$  cm area with thicknesses of 90 and 160 nm. The 90-nm thick films exhibited a thickness variation of  $\pm 8\%$ ,  $T_{\text{co}} = 90.7 \pm 0.5$  K,  $J_c = 4.8 \pm 0.2 \times 10^6$  A/cm<sup>2</sup> at 77 K, and a surface resistance (corrected for finite thickness) at 75 GHz of 10–12 m $\Omega$  at 77 K. For the 160-nm thick films, the thickness variation was  $< 5\%$ ,  $T_{\text{co}} = 91.0 \pm 0.3$  K,  $J_c = 5.4 \pm 0.4 \times 10^6$  A/cm<sup>2</sup>, and corrected surface resistance was 6–10 m $\Omega$ . X-ray diffraction showed that the *c*-axis mosaic in the films is closely related to that of the substrates and that the only in-plane defects are due to the expected twinning in the *a*-*b* plane of the film. The *c*-axis lattice constants were  $1.1688 \pm 0.0004$  nm. The above properties showed a high degree of uniformity across the substrate area and between films from different deposition cycles. The surface resistance values add significantly to the body of results which show that the temperature-scaled values for niobium can be equaled and perhaps surpassed by  $\text{YBa}_2\text{Cu}_3\text{O}_{7-\delta}$ .

## I. INTRODUCTION

Large area, high quality thin films of high- $T_c$  materials are of considerable technological importance in the development of passive and active devices including delay lines, filters, interconnects, and arrays of superconducting quantum interference devices. Large area films of the superconducting compound  $\text{YBa}_2\text{Cu}_3\text{O}_{7-\delta}$  (YBCO) have been fabricated with such techniques as off-axis sputtering,<sup>1</sup> coevaporation,<sup>2</sup> electron beam flash evaporation,<sup>3</sup> and metalorganic chemical vapor deposition.<sup>4</sup> The technique of pulsed laser deposition (PLD) has produced some of the highest quality films to date.<sup>5,6</sup> These films, however, are typically no larger than  $1 \times 1$  cm. One strategy for depositing larger areas by PLD has been to steer a small beam across a large target, which has produced uniform film areas as large as  $1.5 \times 1.5$  cm.<sup>7</sup> Scale-up to areas of  $2.5 \times 2.5$  cm has been mentioned by Wu *et al.*<sup>8</sup> in connection with a high deposition rate study that incorporated substrate rotation. To our knowledge, however, a process for depositing large area, uniform films with state-of-the-art performance has not been published. In this work, we describe thin films deposited in a system where substrates are scanned over areas up to  $3.5 \times 3.5$  cm through a stationary plume of ablated material which is defined by an aperture.

The four main features of the deposition system which

allow for uniform film growth over large areas are the following: line focusing of the laser beam onto the target; an aperture that defines the area of the plume which produces the highest quality material; a computerized, stepper motor-driven *X*-*Y* stage which translates the heated sample holder behind the plume-defining aperture in programmed patterns with  $\pm 0.5$  mm accuracy and repeatability; and a substrate mounting block with uniform heating at high temperatures over large areas.

Line focusing allows for the formation of a relatively large plume having uniform ablatant flux density and correct composition. An aperture has been used to mask the portions of this plume which lead to nonuniform deposits. The dimensions of the aperture were determined empirically, but are consistent with a detailed plume uniformity study.<sup>9</sup> The aperture was placed in close proximity to the substrate to give relatively sharp edges to the per-pulse deposit, thus scanning patterns which yielded uniform film thicknesses were readily determined.

## II. EXPERIMENTAL PROCEDURES

A Questek 2860 excimer laser operating on the 248-nm (KrF) line was used for ablation. This laser has uniform fluence over a beam area of approximately  $1 \times 2.4$  cm. The beam was focused to a  $0.1 \times 2$  cm line having a nominal

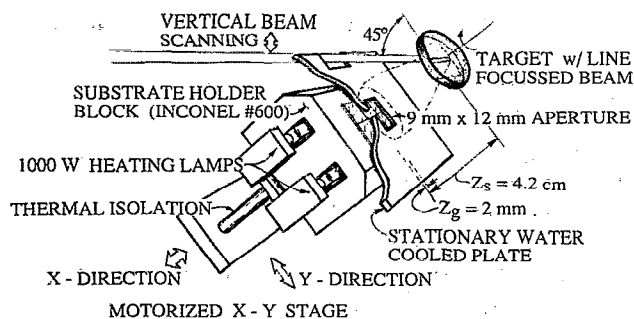


FIG. 1. Diagram of the substrate scanning pulsed laser deposition system.

energy density of  $1.6 \text{ J/cm}^2$  onto a round rotating target 2.5 cm in diameter. The beam was continuously scanned in the vertical direction with a 0.7 cm displacement to randomize beam impingement over a  $45^\circ$  solid angle with respect to target normal. A 90-cm focal length was used, thus limiting energy density variations at the target to  $\pm 8\%$  during scanning. The target was a 90% dense stoichiometric YBCO pellet supplied by the W. R. Grace Co. The relative orientations of the target to the beam and to the aperture are shown in Fig. 1.

The plasma plume yielded deposits uniform in thickness and composition over an area 10 mm in the  $x$ -direction and 15 mm in the  $y$ -direction at a distance of 4.2 cm from the target surface at the 200 mTorr deposition pressure; this was determined by depositing test films on Si wafers without an aperture at room temperature and analyzing them by stylus profiling and energy dispersive x-ray spectrometry. The aperture dimensions that were used were somewhat smaller: 10 mm in the  $x$ -direction and 13 mm in the  $y$ -direction. The aperture was constructed of a thin, water-cooled, copper plate. Water cooling minimized radiant heating of the aperture and target by the large exposed substrate area.

When an expanding plume approaches the aperture plate, relatively high pressure waves rebound from the surface and hole edges which compress the plume that passes through. These waves are probably due to ambient oxygen which is pushed by the plasma front; they have the effect of reducing the effective aperture area to about  $9 \times 12 \text{ mm}$ . Evidence for oxygen being "swept up" has been seen in high speed photography of plume expansions.<sup>10</sup> The plume compression effect we observed was inferred through film thickness profiling of test films deposited through several apertures and with various aperture-substrate spacings ( $z_g$ ): edge thinning occupied a greater fraction of deposit area with increased  $z_g$ . With narrow aperture dimensions (approaching  $z_g$ ), Gaussian-like deposit profiles were produced. The complications imposed on depositing uniformly by this edge effect were reduced by minimizing  $z_g$ , maximizing aperture area, and employing a scanning strategy that would average edge effects uniformly over the entire deposited area.

Scan profiles were serpentine, with movement in the  $x$ -direction continuous, and the position in the  $y$ -direction incremented at the end of each horizontal scan. The quasi-

linear variation of the edge thickness which we observed in the test films using a small  $z_g$  had a range that was about equal to  $z_g$ . Thus a  $y$ -increment one-half of the linear variation range was chosen to ensure that edge thickness variation from the top and bottom of the aperture would overlap and cancel. The extremes of scan position completely removed the substrates from the aperture area. Scan cycles were repeated a number of times to obtain the desired film thickness.

Uniform substrate temperatures over large areas were achieved with a sample holder constructed entirely from a high nickel alloy (Inconel No. 600). The holder has an internal cavity which contains two 1-kW quartz-halogen lamps; these enable it to attain temperatures greater than  $1000^\circ\text{C}$  at full power in atmospheric pressure oxygen. The holder was surrounded, except for a window around the substrate mounting area, with a radiation shield fabricated from two layers of Ni foil. Optical pyrometer measurements across the  $4 \times 4 \text{ cm}$  substrate mounting area showed unmeasurable temperature variation with this shielding at the deposition temperature of  $770^\circ\text{C}$ . Substrates were cemented to the holder with silver paint, which was cured by baking the holder at  $300^\circ\text{C}$  for 30 min and  $770^\circ\text{C}$  for 5 min in air prior to system pumpdown. Process temperature measurement for feedback control was made with a platinum thermocouple imbedded in the sample holder underneath the substrate mounting area. Infrared thermometry measurements of deposited films, using an emissivity correction for the high surface smoothness, confirmed a film surface temperature equal (within  $5^\circ\text{C}$ ) to the bulk of the substrate holder in vacuum.

Two sets of films were deposited in *successive* runs to investigate uniformity over large areas with film thicknesses 90 and 160 nm. Each set or batch of films was deposited on a  $2 \times 3$  array of substrates consisting of two  $1 \times 1 \text{ cm}$  (100)  $\text{SrTiO}_3$  substrates located on opposite corners with the remaining four substrates being  $1 \times 1 \text{ cm}$  (100)  $\text{LaAlO}_3$ . Samples referred to specifically below are 0921c and 0921d, which are from opposite corners of the 90 nm batch, and 0925c and 0925d, which are from opposite corners of the 160 nm batch. All of these numbered samples are on  $\text{LaAlO}_3$  substrates.

Process parameters included an oxygen pressure of 200 mTorr, target-to-substrate spacing ( $z_s$ ) of 4.2 cm, and a cooling ramp rate of  $4^\circ\text{C}/\text{min}$  in pure  $\text{O}_2$  at a pressure of 1 atm. The deposition temperature used was determined in a previous optimization study.<sup>11</sup> Target preparation consisted of sanding with No. 600 sandpaper and rinsing in acetone prior to pumpdown. Substrates were then shielded and the target was preblated for 10 min at 10 Hz with continuous beam scanning, at the base pressure of  $< 1 \text{ mTorr}$ . Film growth was then initiated with a horizontal scanning rate of  $2.54 \text{ mm/s}$  and a laser pulse repetition rate of 23.5 Hz through the effective 9-mm wide aperture. Each pulse contributed about 0.05 nm to the film thickness and the net deposition was about 4 nm/horizontal scan. The  $z_g$  for these depositions was 2 mm and, as discussed above, the vertical scan increment of 1 mm was used. The effective vertical dimension of the aperture was 12 mm and, there-

fore, an entire scan cycle required 32 horizontal scans. The scan time for each cycle was approximately 9 min, and the net deposited film thickness per cycle was between 40 and 50 nm.

Resistive transitions were measured by an ac four-point technique with a lock-in amplifier with a sensitivity limit of  $10^{-5}$   $\Omega$ . The  $T_{co}$  values we report correspond to the temperature at which the noise limit was achieved. The differential resistance ( $dV/dI$ ) of patterned bridges at 77.1 K was measured as the voltage response to a low-amplitude ac current excitation while applying various levels of dc current ( $I$ );  $I$  was applied in 100 ms pulses to minimize contact heating. The resulting  $dV/dI$  vs  $I$  curves were numerically integrated to give the  $I$ - $V$  characteristic. The critical current  $I_c$  was defined as the current axis intercept of a tangent line drawn on the  $I$ - $V$  curve at 100 nV, which corresponds to an electric field of 1  $\mu$ V/cm. This value of electric field is a factor of 10 smaller than the value suggested by the National Institute of Standards and Technology,<sup>12</sup> but, due to the steepness of the  $I$ - $V$  curve, makes very little difference to the measured value of  $I_c$ . Bridge dimensions were 2, 5, 10, and 20  $\mu$ m  $\times$  1 mm, and were fabricated by photolithography using Olin-Hunt HNR 120 negative tone resist and Ar<sup>+</sup> ion milling. Because the etching process produced faceted sidewalls, area cross sections of the 2, 5, and 10  $\mu$ m lines were calculated from the measured room-temperature resistivity of the 20  $\mu$ m line on each film. We have determined previously that resistivity is constant across films made with this process. Film thickness was determined to an accuracy of  $\pm 5\%$  by breaking samples and viewing them in profile in a scanning electron microscope (SEM).

The structure of the four numbered samples was characterized by x-ray diffraction (XRD). A Siemens D5000 diffractometer with a Cu anode and a curved graphite diffracted beam monochromator was employed to collect (00L) intensities and to perform  $\omega$ -scans of film (005) and substrate (200) reflections.

Films were aligned by first performing  $\omega$ -scans of the LaAlO<sub>3</sub> substrate, and resetting  $\omega$  so that at the peak position,  $\omega = 2\theta/2$ . Standard  $\theta$ - $2\theta$  scans were then performed and the  $c$ -axis lattice constants were calculated from the (00L) reflections. Next,  $\omega$ -scans of the (005) reflection were performed to determine the mosaic of the film. Finally,  $\omega$ -scans of the (200) LaAlO<sub>3</sub> reflection were measured to determine the mosaic of the substrates.

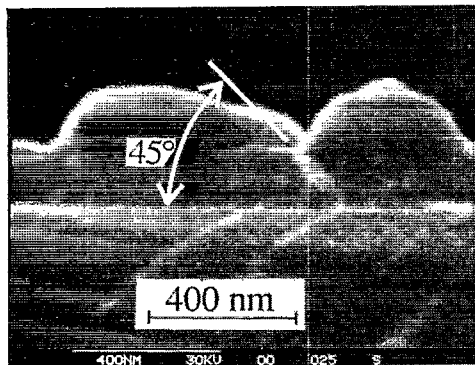
The in-plane texture of the films was analyzed using a pole figure attachment.<sup>13</sup> With  $\chi = \phi = 0^\circ$ , films were aligned using the same procedure as for the (00L) scans. In order to ensure that there was only one  $c$ -axis orientation, a pole figure was first taken about the (005) reflection. This was done by starting with  $\chi = \phi = 0.0^\circ$ ,  $\omega = 19.25^\circ$ ,  $2\theta = 38.49^\circ$ , and scanning in  $\phi$  from  $\phi = 0.0^\circ$  to  $360.0^\circ$  using  $1^\circ$  steps. In the pole figure configuration, the angular acceptance of the detector was sufficiently large to allow for a  $1^\circ$  step size in  $\phi$  and  $\chi$ . For the (213) pole figure the same procedure was followed, using initial starting angles of  $\phi = 0.0^\circ$ ,  $\omega = 29.42^\circ$ , and  $2\theta = 58.83^\circ$ . Full  $360^\circ$

scans in  $\phi$  were taken at  $1^\circ$  increments of  $\chi$  over the range of  $60^\circ$ - $80^\circ$ .

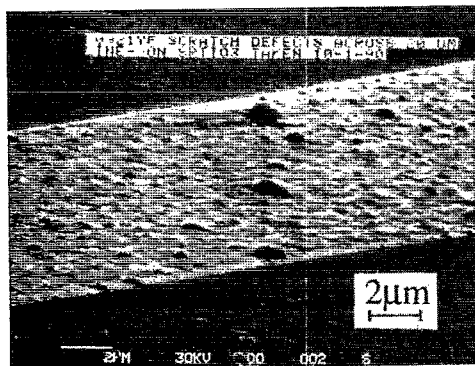
Microwave properties of the four numbered films were characterized by measurements of surface resistance ( $R_s$ ). Measurements of the unloaded quality factor  $Q$  were taken for a  $TE_{011}$  cylindrical copper cavity where the sample replaced one of the endplates. These measurements were performed at 75 GHz using an HP8510 network analyzer and a modification of Ginzton's impedance method.<sup>14</sup> A description of the apparatus and formulas used in calculation of  $R_s$ , as well as a complete analysis of the sensitivity of this method, are described elsewhere.<sup>15</sup>

Geometrical factors for the all copper cavity  $\Gamma_0$  and the all copper cavity without one endplate  $\Gamma_{max}$  were calculated as 745 and 910  $\Omega$ , respectively, using the known ratio of the cavity diameter to its height. Consequently, the ratio of  $\Gamma_{max}/\Gamma_0$  was 1.22. For experimental verification of the calculated factors  $\Gamma_0$  and  $\Gamma_{max}$ , we measured the dc resistivity  $\rho$  ( $2.62 \pm 0.05$   $\mu\Omega$  cm at 300 K) of a sample made from the same piece of oxygen free high conductivity copper which was used to make the cavity. The surface of the sample was prepared in the same way as the surface of the cavity.  $R_s$  was calculated using the relation  $R_s = (\pi f \mu_0 \rho)^{1/2}$  where  $f$  is the frequency and  $\mu_0$  is the permeability of space. By measuring the  $Q_{0Cu}$  of the all copper cavity at 300 K, the experimental geometrical factor  $\Gamma_0$  was found to be  $729 \pm 18$   $\Omega$ , a result which agrees with the calculated value to within the measurement error. To find the experimental ratio of  $\Gamma_{max}/\Gamma_0$ ,  $Q_{max}$  at 4.2 K was measured by using a Nb thin film as the endplate. Combining this with a measurement of  $Q_{0Cu}$  at 4.2 K gives the measured ratio  $\Gamma_{max}/\Gamma_0 = 1.21$ . This result is also in very good agreement with the value expected based on the calculations. The  $Q_{max}/Q_{0Cu}$  ratio determines the sensitivity limit (defined as the value of  $R_s$  where the standard error is 50% of the measured value) of the cavity, which is about 0.15  $R_s$  of copper (about 7 m $\Omega$  at 77 K).<sup>14</sup>

The  $R_s$  of films having thicknesses on the order of the penetration depth ( $\lambda$ ) or less has an effective or measured value which is larger than the intrinsic value. This increase depends on the film thickness and dielectric properties of the substrate.<sup>16</sup> In a sample much thicker than the penetration depth, both magnetic fields and currents decay exponentially from the sample surface. However, assuming that the external magnetic rf field remains constant, as the thickness of the sample is decreased to dimensions on the order of  $\lambda$ , the current becomes more uniform and the net current density in the sample increases. The increased current density results in an increase in the effective  $R_s$ . Substrate absorption and transmission losses also increase the effective surface resistance of very thin films. In very thin films, such as those measured here, the current density becomes almost uniform throughout the thickness of the film,<sup>17</sup> and measured values can be many times greater than the intrinsic values. Intrinsic values of  $R_s$  were calculated using formula (8a) of Ref. 15. The  $a$ - $b$  plane values of the magnetic penetration depth used to evaluate the corrections to  $R_s$  were 260 nm (77 K) and 140 nm (4.2 K).<sup>18</sup>



(a)



(b)

FIG. 2. (a) Scanning electron micrograph of two outgrowths in a 160-nm thick film exposed by breaking the substrate and viewing edge-on. The  $45^\circ$  angle between the base of the outgrowth and the plane of the film is shown. Film thickness is readily determined from the scale (160 nm), (b) large outgrowths aligned with substrate scratches in  $20\ \mu\text{m}$  wide, 90 nm thick line on  $\text{SrTiO}_3$ .

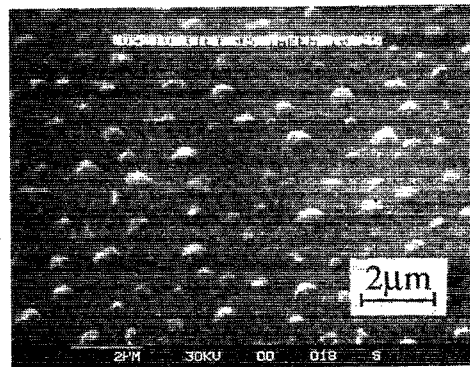
### III. RESULTS

#### A. Transport properties

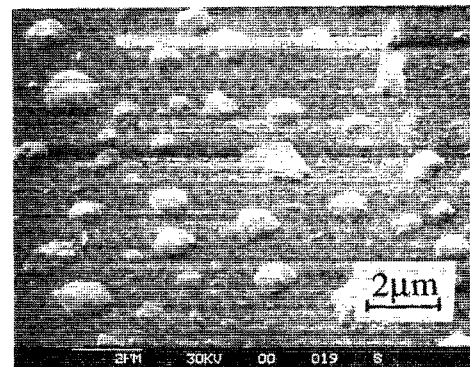
Resistive transitions and critical current densities were consistent in all samples. In the 90-nm thick batch, the  $T_{c0}$  values ranged from 90.2 to 91.2 K; in the 160-nm thick batch, the range was 90.7–91.3 K.  $J_c$  was measured on at least two lines on each of three films of each batch. In the 90 nm batch, the mean value of  $J_c$  was  $4.8 \times 10^6\ \text{A/cm}^2$  with a standard deviation ( $\sigma$ ) of  $0.2 \times 10^6\ \text{A/cm}^2$ . In the 160 nm batch, the mean value was  $5.4 \times 10^6\ \text{A/cm}^2$  and  $\sigma$  was  $0.4 \times 10^6\ \text{A/cm}^2$ . In both  $T_c$  and  $J_c$  results, there was no significant difference between films on  $\text{SrTiO}_3$  and  $\text{LaAlO}_3$  substrates, and there was no linewidth dependence in  $J_c$ . The room-temperature resistivity was  $238\ \mu\Omega\ \text{cm}$  in the 90 nm films and  $227\ \mu\Omega\ \text{cm}$  in the 160 nm films.

#### B. Morphological characteristics

Thickness uniformity, measured by viewing a broken edge in a SEM, indicated that variations across the 90 nm batch were about 8%, and that variations were unmeasurable in the 160 nm batch. The variation in the 90 nm batch was due to a failure of target scanning by the laser beam steering mirror during deposition. The edge views also revealed that “bumps” or outgrowths tend to grow at a ver-



(a)



(b)

FIG. 3. (a) Scanning electron micrograph of a typical 90 nm thick film viewed at a  $45^\circ$  angle, (b) surface of typical 160 nm thick film [same magnification and angle as in (a)].

tical rate which is at least twice that of the surrounding film, as indicated by their relative height. They nucleate at sites of various sizes on the substrate surface and grow in an inverted conical or pyramidal geometry which has an included angle of approximately  $90^\circ$ . This is shown in Fig. 2(a), where the base of a cone in a 160-nm thick film was exposed when the substrate was broken. This regular subsurface geometry suggests that they are crystalline, that their lateral growth rate equals that of the vertical growth rate of the surrounding film, and finally, that they are *not* the result of particulate ejection from the target during growth. For reasons discussed below, however, we cannot unambiguously state that they are *a*- or *b*-normal oriented domains of YBCO material, as has been observed by Chang *et al.* in a recent study.<sup>19</sup> We have observed that they tend to decorate obvious defects in the substrate. This is shown in Fig. 2(b), where unusually large outgrowths are aligned with parallel microscratches which are about as deep as the thickness of the film.

The number density and diameter of the outgrowths vary with the film thickness; in the 90-nm thick batch the density was approximately  $0.57\ \mu\text{m}^{-2}$  and the mean diameter was  $0.46\ \mu\text{m}$ . In the 160-nm thick batch, the density was *lower*, at  $0.27\ \mu\text{m}^{-2}$ , while the mean diameter was greater, at  $0.88\ \mu\text{m}$ . These numbers were determined from examination of SEM micrographs, such as those in Figs. 3(a) and 3(b), which are representative of the two batches. This density reduction with increased film thick-

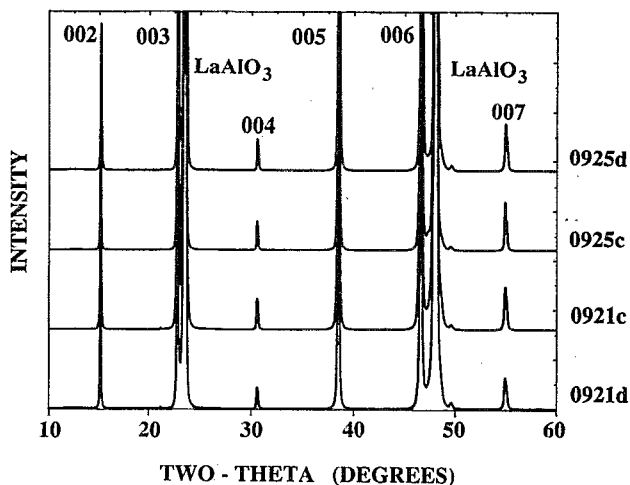


FIG. 4. Comparison of  $\theta$ - $2\theta$  data of four numbered films on  $\text{LaAlO}_3$ .

ness is consistent with a result of Chang.<sup>19</sup> We can now add that the density and diameter of outgrowths do not vary between samples on  $\text{SrTiO}_3$  and  $\text{LaAlO}_3$  substrates deposited under identical conditions, indicating that nucleation site densities and sizes are substrate independent.

### C. Crystallographic structure

The (00L) scans that were taken clearly show that each of the four numbered films consist of  $c$ -axis oriented grains, as shown in Fig. 4. Since  $a$  is nearly equal to  $c/3$ , any small  $a$ -normal oriented grains would not be detected in the (00L) scans with this diffractometer resolution. Similarly,  $b$ -normal oriented grains would not be easily detected, because the  $\text{LaAlO}_3$  substrate reflections are very intense, relatively broad, and appear close to the expected  $2\theta$  position of film (0 $k$ 0) reflections. At this time we cannot therefore comment as to the fraction of film having  $a$ - or  $b$ -axis normal orientation.

The intensities of the (00L) reflections scaled with film thickness as expected. The (007) reflection of the 160 nm thick films in particular show  $K\alpha_1 - K\alpha_2$  splitting, which is a good indication that there are at most only minor stacking faults along the  $c$ -axis. More detailed modeling is required to quantify this point, however. The  $c$ -axis lattice constants of the four films are given in Table I; they are identical within experimental error.

Rocking curve structure and peak widths for the (005) YBCO reflection and the (200)  $\text{LaAlO}_3$  reflection are similar, as shown in Figs. 5(a) and 5(b) (sample 0925d). It is

TABLE I. Properties of numbered films.

Sample No.	Thickness (nm)	$c$ -lattice constant (nm)	Measured $R_s$ (m $\Omega$ )	$R_s$ , 77 K (m $\Omega$ )	$R_s$ , 4.2 K (m $\Omega$ )
0921c	90	$1.1691 \pm 0.0004$	75	13	2
0921d	97	$1.1688 \pm 0.0004$	55	10	2
0925c	160	$1.1686 \pm 0.0004$	31	10	<2
0925d	160	$1.1691 \pm 0.0004$	21	6	<2

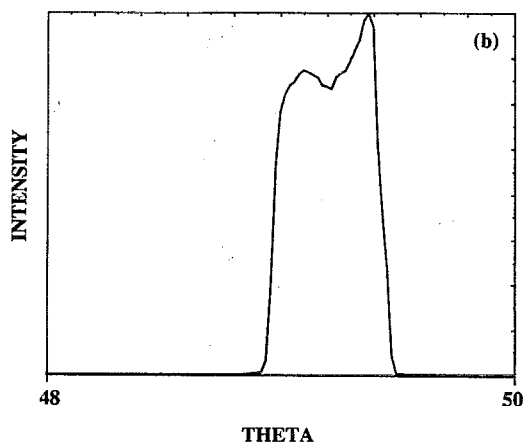
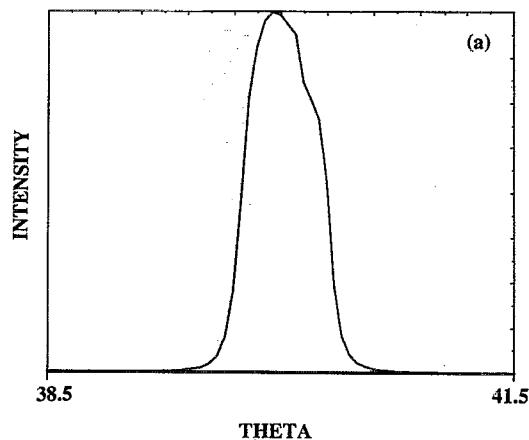


FIG. 5. (a) The  $c$ -axis mosaic of a 160 nm film ( $\omega$ -scan of (005) YBCO peak), (b) the  $x$ -axis mosaic of the  $\text{LaAlO}_3$  substrate for the film in (a) [ $\omega$ -scan of (200) peak].

apparent that the substrate [Fig. 5(b)] consists of two large mosaic blocks, and that the film [Fig. 5(a)] has this same two mosaic block structure. These blocks are indicated by the two-peak structure. As expected with a thin *epitaxial* film, the mosaic structure of the substrate is mimicked in the film. We note that the  $c$ -axis mosaic of these films are limited by the quality of the substrate material.

Pole figures taken about the (213) reflection for one film from each batch are shown in Fig. 6. If all the grains were oriented in the film plane, with each having the same  $a$ -axis orientation, then we would expect to see 4 poles. However, for each of these films, we found 8 poles. These pole positions are consistent with a model where the film consists of grains with two perpendicular  $a$ -axis orientations, both in the plane. There are no apparent differences between the pole figures of any of the four films, and there was no evidence of  $45^\circ$  grains.

### D. Millimeter-wave surface resistance

Figure 7 shows the effective surface resistance versus temperature for all four of the measured films, and also that of a  $0.5\text{-}\mu\text{m}$  thick Nb film. The results obtained for films within each batch are similar, though not identical.

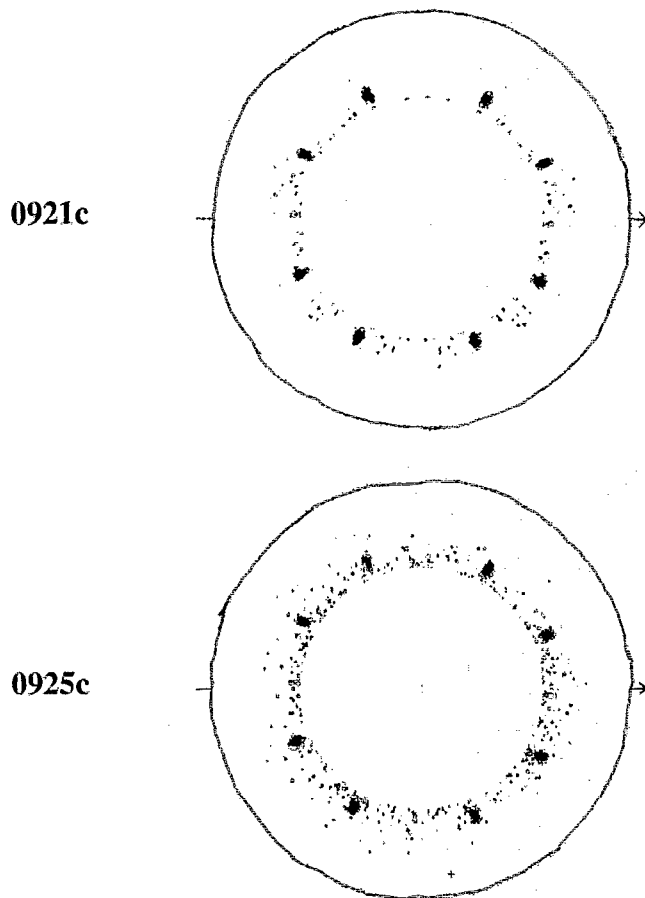


FIG. 6. Pole figures of the (213) reflections for one 90 nm film (top) and one 160 nm film.

The difference between the batches is much larger, but is expected, as discussed above, on the basis of differing film thickness. The values of  $R_s$  corrected for finite thickness at 77 and 4.2 K are listed in Table I. Values below 2 m $\Omega$  exceed experimental sensitivity for the corrected surface resistance.

#### IV. DISCUSSION

The high degree of uniformity of properties in each film batch illustrates that PLD can be applied to produce large YBCO films of the highest quality. The described process has proven to be extremely reproducible, having given 100% yields with films of this or better quality over as many as 12 consecutive runs. We see no impediment to further scale-up, although larger areas will require higher pulse repetition rates as well as faster substrate scanning so as to limit local growth rates to epitaxial coalescence limits of about 7 nm/s, as reported by Wu *et al.*<sup>8</sup>

The reduction of outgrowth size and density in larger films may be difficult if the formation rate of outgrowth nuclei increases under the necessary conditions of high local growth rate and long intervening periods of annealing. Annealing periods will exceed tens of minutes between scan cycles with significantly larger areas, unless all parameters (i.e., target/uniform plume size) can be appropriately

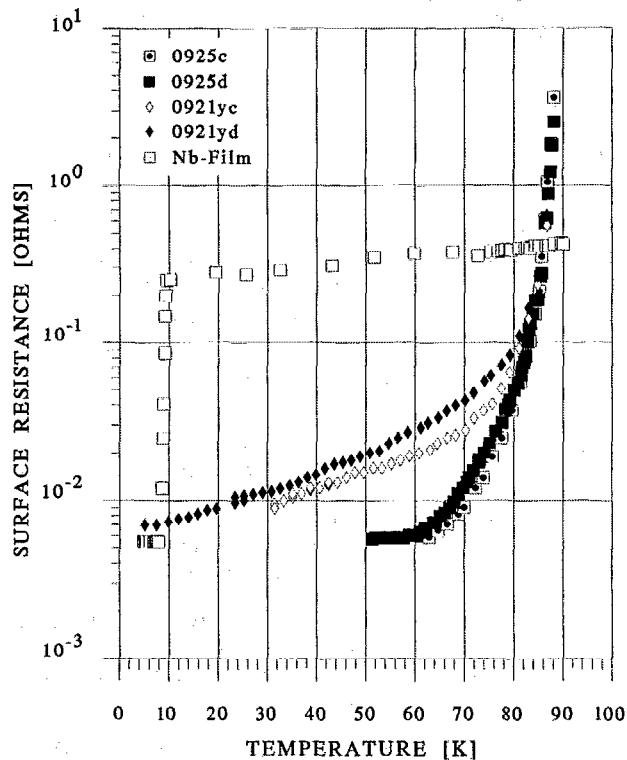


FIG. 7. Comparison of measured  $R_s$  for the four numbered films and for a Nb film.

scaled. The results of Chang *et al.*<sup>19</sup> suggest that an onset of outgrowth formation occurs at a net deposition rate between 1.5 and 4.2 nm/s (with a per-pulse deposit of about 0.16 nm/shot). Our results show similar outgrowth formation, but at a lower rate of 1.2 nm/s and a lower deposited thickness per pulse of about 0.05 nm. The difference in thresholds is probably due to our higher deposition temperature.

These films are qualitatively best described as being small single crystals carefully set down as if laying tiles on the substrate, and in this tiling, only two  $a$ -axis in-plane orientations exist. From the data taken, however, we cannot comment on the extent of the domains associated with either orientation, or on crystallite size. These are probably closely correlated to the extensive twinning and the broad mosaic of the LaAlO<sub>3</sub> substrate material. We were unable to take detailed diffraction data on the SrTiO<sub>3</sub> samples to clarify this point, however. Structurally, all films of a given thickness are indistinguishable: every small feature in the diffraction data for one film is found in the data for every other.

The values for 75 GHz surface resistance, corrected for finite thickness, are near 10 m $\Omega$  at 77 K. This is important confirmation of the value of 8 m $\Omega$  reported by Klein *et al.*<sup>20</sup> and by ourselves,<sup>11</sup> which show that YBCO can approach the performance of temperature-scaled niobium (6 m $\Omega$  at 7.7 K). These low values of  $R_s$  are consistent with a very preliminary upper bound value of 2.6  $\Omega$  at 1.4 THz and 77 K, which was obtained using laser reflectometry on one of our 2 cm  $\times$  2 cm  $\times$  400 nm thick films.<sup>21</sup> This

result corresponds to an  $f^2$ -scaled value of 7.5 m $\Omega$  at 75 GHz.

## ACKNOWLEDGMENTS

The authors would like to thank D. Elthon, J. Miller, and T. Robin for helpful conversations and suggestions, N. Spencer of the W. R. Grace Co. for providing high quality ablation targets, and Questek for excellent hardware support. The work was supported by the State of Texas through the Texas Center for Superconductivity, by NASA Grant NAG-9-352 and, in its early stages, by DARPA Grant MDA 972-88-G-0002.

- <sup>1</sup>N. Newman, K. Char, S. M. Garrison, R. W. Barton, R. C. Taber, C. B. Eom, T. H. Geballe, and B. Wilkens, *Appl. Phys. Lett.* **57**, 520 (1990).
- <sup>2</sup>P. M. Mankiewich, J. H. Scofield, W. J. Skocpol, R. E. Howard, A. H. Dayen, and E. Good, *Appl. Phys. Lett.* **51**, 1753 (1987).
- <sup>3</sup>M. F. Davis, J. L. Wosik, and J. C. Wolfe, *J. Appl. Phys.* **66**, 4903 (1989).
- <sup>4</sup>J. M. Zhang, H. O. Marcy, L. M. Tonge, B. W. Wessels, T. J. Marks, and C. R. Kannewurf, *Appl. Phys. Lett.* **55**, 1906 (1989).
- <sup>5</sup>D. Dijkkamp, T. Venkatesan, X. D. Wu, S. A. Saheen, N. Jisrawi, H. H. Min-Lee, W. L. McLean, and M. Croft, *Appl. Phys. Lett.* **51**, 619 (1987).
- <sup>6</sup>T. Venkatesan, X. D. Wu, B. Dutta, A. Inam, M. S. Hedge, D. M. Hwang, C. C. Chang, L. Nazar, and B. Wilkens, *Appl. Phys. Lett.* **54**, 1054 (1989).
- <sup>7</sup>G. Koren, A. Gupta, E. A. Geiss, A. Segmuller, and R. B. Laibowitz, *Appl. Phys. Lett.* **54**, 1054 (1989).

- <sup>8</sup>X. D. Wu, R. E. Muenchausen, S. Foltyn, R. C. Estler, R. C. Dye, C. Flamme, N. S. Nogar, A. R. Garcia, J. Martin, and J. Tesmer, *Appl. Phys. Lett.* **56**, 1481 (1990).
- <sup>9</sup>R. E. Muenchausen, K. M. Hubbard, S. Foltyn, R. C. Estler, N. S. Nogar, and C. Jenkins, *Appl. Phys. Lett.* **56**, 579 (1990).
- <sup>10</sup>K. Scott, J. M. Huntley, W. A. Phillips, J. Clarke, and J. E. Field, *Appl. Phys. Lett.* **57**, 922 (1990).
- <sup>11</sup>J. Wosik, T. Robin, M. F. Davis, J. C. Wolfe, K. Forster, S. Deshmukh, A. Bensaoula, R. Sega, D. Economou, and A. Ignatiev, *Proceedings of the Second Conference on the Science and Technology of Thin Film Superconductors*, Denver, CO, April 30-May 4, 1990, edited by R. D. McConnell and R. Noufi (to be published).
- <sup>12</sup>J. W. Ekin, *Appl. Phys. Lett.* **55**, 905 (1989).
- <sup>13</sup>C. S. Barrett and T. B. Massalski, *Structure of Metals* (Pergamon, New York, 1980).
- <sup>14</sup>D. Kajfez and E. J. Hwan, *IEEE Trans. Microwave Theory Techn.* **MTT-32**, 666 (1984).
- <sup>15</sup>J. Wosik, R. A. Kranenburg, J. C. Wolfe, V. Selvamanickam, and K. Salama, *J. Appl. Phys.* **69**, 874 (1991).
- <sup>16</sup>N. Klein, H. Choloupka, G. Müller, S. Orbach, and H. Piel, *J. Appl. Phys.* **67**, 6940 (1990).
- <sup>17</sup>S. Shridar, *J. Appl. Phys.* **63**, 159 (1988).
- <sup>18</sup>A. T. Fiory, A. F. Hebard, P. M. Mankiewich, and R. E. Howard, *Phys. Rev. Lett.* **61**, 1419 (1988).
- <sup>19</sup>C. C. Chang, X. D. Wu, R. Ramesh, X. X. Xi, T. S. Ravi, T. Venkatesan, D. M. Hwang, R. E. Muenchausen, S. Foltyn, and S. Nogar, *Appl. Phys. Lett.* **57**, 1814 (1990).
- <sup>20</sup>N. Klein, G. Müller, H. Piel, B. Roas, L. Schultz, U. Klein, and M. Peiniger, *J. Appl. Phys.* **54**, 757 (1989).
- <sup>21</sup>P. P. Woskov, D. R. Cohn, S. C. Han, R. H. Giles, and J. Waldman, *Proceedings of the 15th International Conference on Infrared and Millimeter Waves*, Orlando, FL, December 10-14, 1990, edited by R. J. Temkin (to be published).